Effect of a Phonon Bottleneck on Exciton and Spin Generation in Self-Assembled $In_{1-x}Ga_xAs$ Quantum Dots

Y. Q. Huang,[1] I. A. Buyanova,[1] X. J. Yang,[3] A. Murayama,[2] and W. M. Chen[1]

[1]*Department of Physics, Chemistry and Biology, Linköping University, S-581 83 Linköping, Sweden*
[2]*Graduate School of Information Science and Technology, Hokkaido University, Kita 14, Nishi 9, Kita-ku, Sapporo 060-0814, Japan*
[3]*Suzhou QiangMing Optoelectronics, Co. Ltd., Suzhou 215-028, Jiangsu, China*

(Received 17 November 2017; revised manuscript received 1 February 2018; published 26 April 2018)

We provide direct experimental evidence for the effect of a phonon bottleneck on exciton and spin generation in self-assembled $In_{0.5}Ga_{0.5}As$ quantum dots (QDs). With the aid of tunable laser spectroscopy, we resolve and identify efficient exciton generation channels in the QDs mediated by longitudinal-optical (LO) phonons from an otherwise inhomogeneously broadened QD emission background that suffers from the phonon bottleneck effect in exciton generation. Spin-generation efficiency is found to be enhanced under the LO-assisted excitation condition due to suppressed spin relaxation accompanying accelerated exciton generation. These findings underline the importance of fine-tuning QD energy levels that will benefit potential spin-optoelectronic applications of QDs by reducing spin loss due to the phonon bottleneck.

DOI: 10.1103/PhysRevApplied.9.044037

I. INTRODUCTION

Owing to three-dimensional confinement, electronic or excitonic states inside a semiconductor quantum dot (QD) exhibit discrete energy levels [1–4]. Such localized stationary states combined with their large oscillator strengths promise great potential for applications in, e.g., solid-state light-emitting devices and optical quantum-information technology. Indeed, over the last decades, high-quality light-emitting diodes (LEDs), lasers, and single-photon sources have been demonstrated from such quasi-zero-dimensional systems showing superior performance over traditional higher-dimensional materials [5–8]. The discreteness of the QD electronic states also favors a prolonged spin-relaxation time, as the common spin-relaxation processes involving spin-orbit coupling are strongly suppressed [9–11]. Such advantage has aroused interest in extensive research on employing QDs as basic building blocks of spintronics and has led to great progress over the past years in understanding and control of the spin properties in QDs. For instance, efficient initialization, manipulation, and readout of ground-state spin information were achieved in various QDs, and the idea of spin-polarized LEDs has been proposed and put to test [12–15].

Despite the aforementioned advantages, one inherent problem with QDs is inefficient carrier and exciton relaxation via multiple acoustic phonon emissions between discrete energy levels. This arises from a lack of efficient cascade momentum relaxation within a continuum energy band that is available in a higher-dimensional system. This so-called phonon bottleneck has been previously addressed as a fundamental limitation that inhibits efficiency and operation speed of QD devices [16]. On the other hand, it was also reported recently that carrier-relaxation processes can be dominated by an intradot Auger process, which overcomes the phonon bottleneck under a high-excitation-density condition and results in a fast carrier capture and relaxation process of the order of tens of picoseconds [17]. Although the significance of the phonon bottleneck is still under debate, its effect has indeed been observed experimentally. Suemune and co-workers reported the longitudinal-optical (LO) phonon-assisted carrier relaxation in CdS QDs, underlining the importance of energy conservation for efficient carrier relaxation [18]. Urayama *et al.* determined a carrier-relaxation time of 750 ps in self-assembled $In_{1-x}Ga_xAs$ QDs, which is 1 order of magnitude longer compared with a typical Auger process [19], implying that it is the phonon bottleneck rather than the Auger process that is the governing factor. These results suggest that at a low and moderate excitation level before the Auger process becomes significant, the phonon bottleneck plays a key role in carrier and exciton generation in QDs. Unlike the energy relaxation, which has been discussed intensely in the past, very little is known about spin-relaxation processes in the presence of the phonon bottleneck. Such information is essential to efficient spin generation in QDs and will provide a useful guideline for the design of QD spin LEDs with improved brightness and emission polarization.

In this work, we study exciton and spin generation in the QD exciton ground state (GS) in self-assembled $In_{0.5}Ga_{0.5}As$ QDs samples. By carefully selecting excitation and/or detection energy, thereby tuning the excitation

photon energy either on resonance or off resonance at an integer number of the LO-phonon energies above the exciton GS, we are able to distinguish between the QD ensembles that suffer from the phonon bottleneck and those that undergo more efficient LO-phonon-assisted relaxation. This allows us to directly evaluate the degree of the phonon bottleneck effect on the exciton and spin generation from the ratios of photoluminescence (PL) intensity and circular polarization degree of the QD exciton GS between these two energy relaxation channels.

II. EXPERIMENTAL CONDITIONS

The investigated samples are a set of self-assembled $In_{0.5}Ga_{0.5}As$ QDs that are coupled to an $In_{0.1}Ga_{0.9}As$ quantum well (QW) through tunneling. The QDs have an average lateral diameter of 20 nm and a height of 5 nm before the GaAs capping layer is deposited. Scanning electron microscopy reveals the dot density of around 2×10^{10} cm^{-2}. The QW has a thickness of 20 nm and is separated from the QD layer by a thin GaAs tunneling barrier. The barrier thickness is 4, 6, and 8 nm for the three samples studied. As a similar phonon bottleneck effect is observed in all samples regardless of their tunneling barrier thickness, we present below the representative results from the sample with a 4-nm-thick barrier. The indium alloy content is estimated to be about 50% inside the QDs and 10% in the QW. Sketches of the sample structure and the energy alignment are shown in Figs. 1(a) and 1(b), respectively. The detailed growth conditions can be found in Ref. [20]. We note that the same structure has previously been examined as a promising candidate for spin-LED applications owing to the ultrafast and high-fidelity spin injection between the QW exciton states and a QD excited state (ES). Our present work on the exciton and spin relaxation down to the QD GS is, therefore, not only of fundamental interest but also relevant to possible applications [20,21].

In PL and PL excitation (PLE) experiments, a wavelength-tunable Ti:sapphire laser is used as an optical excitation source with a beam spot size of approximately 1 μm, and the resulting PL is detected in the backscattering geometry using a confocal microscope. In the optical orientation experiments, the excitation laser light is circularly polarized by using a $\lambda/4$ plate, and the resulting PL polarization is obtained by $P_{PL} = [(I^{\sigma^+}_{PL} - I^{\sigma^-}_{PL})/(I^{\sigma^+}_{PL} + I^{\sigma^-}_{PL})]$. Here, $I^{\sigma^+}_{PL}$ and $I^{\sigma^-}_{PL}$ denote the intensities of the σ^+ and σ^- components of the PL emission.

III. RESULTS AND DISCUSSION

A. Photoluminescence and photoluminescence excitation

Figure 1(c) shows representative PL spectra from the studied structures measured at a low temperature under the excitation with a photon energy of 1.55 eV, i.e., slightly above the GaAs band-gap energy. At a relatively low excitation power ($P_{exc} = 1.3 \times 10^5$ W cm^{-2}), only the exciton GS emission band from the QD ensemble peaking at 1.25 eV with broadening of 53 meV is observed. (Because of the high density of the QDs, no sharp lines from individual QD emissions are resolved here.) The observed broadening of the GS emission arises from the variations in size, strain, indium composition, etc., between different QDs, such that a part of the PL band corresponds to a selective fraction of the QD ensemble. With increasing

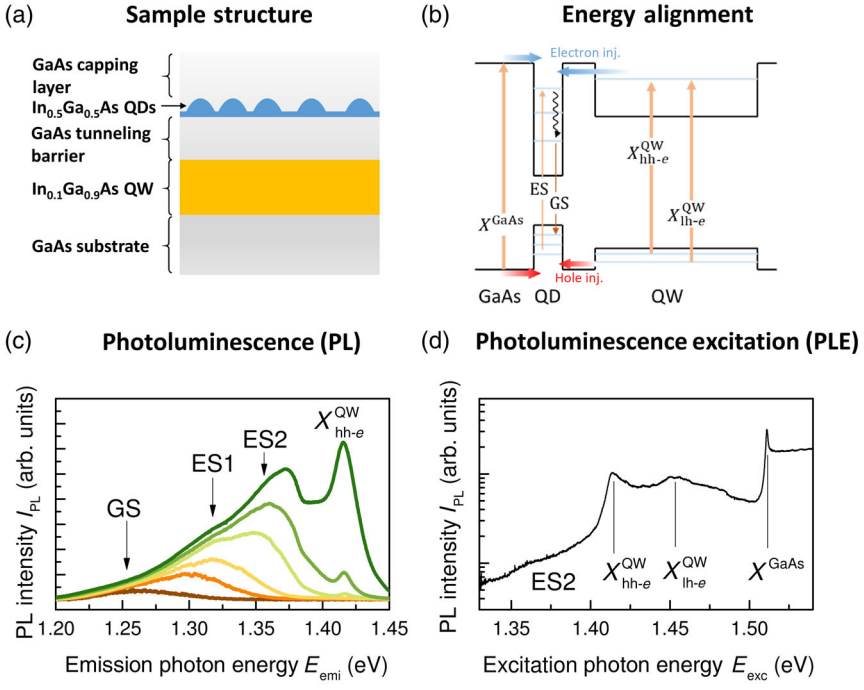

FIG. 1. (a) A sketch of the QD structures studied in this work. (b) The energy alignment of the structures showing the available optical transitions and generation channels of the QD GS exciton. (c) Representative PL spectra from the structures measured at 5 K under the excitation with the photon energy of 1.55 eV above the GaAs band gap. The excitation power density changes from 1.3×10^5 W cm^{-2} for the lowest curve to 1.8×10^7 W cm^{-2} for the highest curve. The optical transitions related to the exciton GS and excited states (ES1 and ES2) of the QDs, as well as the exciton ground state from the QW are identified. (d) PLE spectrum measured at 5 K by detecting the PL emission at the energy of 1.24 eV. The optical absorption features related to the hh-e and lh-e of the QW, and the band-edge exciton of GaAs are marked as $X^{QW}_{hh\text{-}e}$, $X^{QW}_{lh\text{-}e}$, and X^{GaAs}, respectively.

excitation density, the first and second excited states of the QD excitons (labeled as ES1 and ES2) can also be populated with a similar broadening effect. Their average energies are estimated from spectral deconvolution to be 1.32 and 1.36 eV, respectively. At the highest excitation power of 1.8×10^7 W cm^{-2}, the exciton emission from the QW becomes pronounced in the PL spectrum. Its emission energy of 1.415 eV is similar to the heavy-hole exciton (hh-e) transition $X^{\mathrm{QW}}_{\text{hh-}e}$ uncovered from the PLE spectrum shown in Fig. 1(d) obtained by detecting at the low-energy side of the QD GS emission. From the PLE spectrum, it is evident that the exciton generation in the QDs can be accomplished by generating excitons (corresponding to the PLE peaks) and free carriers (corresponding to the continuum in the PLE spectrum) in the GaAs barrier and the QW, as well as by resonant excitation within the QDs without involving the GaAs barrier and the QW. As these different excitation channels are well separated in energy, their role in exciton and spin generation can be addressed separately and individually. In the present study, we employ the experimental conditions with the excitation energy below $X^{\mathrm{QW}}_{\text{hh-}e}$ and at a low-moderate excitation density, such that the phonon bottleneck effect can be selectively examined.

B. Selective PL and PLE

Figure 2(a) shows normalized PL spectra of the QD ensemble at a given excitation photon energy E_{exc}. They are labeled from "A" to "F" with their corresponding excitation energies tuned from above to below $X^{\mathrm{QW}}_{\text{hh-}e}$, as marked in the PLE spectrum given in Fig. 2(b). Different from the PL spectra shown in Fig. 1(c), a much lower excitation power density of 255 W cm^{-2} is used such that only the exciton GS is expected to be occupied. This is because such excitation is expected to lead to an average occupancy of 1.0 and 0.1 electrons or holes per dot for above and below the $X^{\mathrm{QW}}_{\text{hh-}e}$ excitation, respectively, if the exciton lifetime of the QDs is assumed to be 1 ns. The low excitation power guarantees that the Auger process is well suppressed and the carrier or exciton energy relaxation inside the QDs will be generally limited by the slow acoustic phonon process, creating a phonon bottleneck condition. Upon optical excitation of the QW with E_{exc} above $X^{\mathrm{QW}}_{\text{hh-}e}$, e.g., spectra A and B in Fig. 2(a), the PL spectra show a typical and identical emission band with a Gaussian-like line shape that reflects a statistical distribution of the exciton GS energy of the QD ensemble. This finding indicates that the carriers or excitons injected from the QW are sufficiently relaxed down to the QD GS before they emit light and the relaxation is uniform in energy, such that no excess energy remains, nor will there be any preferred QD of whose relaxation time dramatically deviates from the average. When E_{exc} is tuned below $X^{\mathrm{QW}}_{\text{hh-}e}$ (spectra C-F), on the other hand, new features emerge on

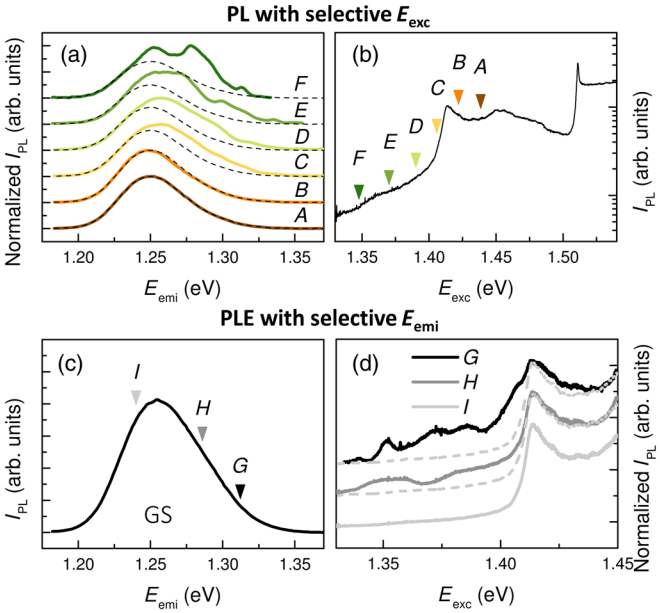

FIG. 2. (a) Normalized PL spectra measured from the QD ensemble by changing the excitation energy from above to below $X^{\mathrm{QW}}_{\text{hh-}e}$. The excitation energies for spectra A–F are indicated in (b). The dashed lines represent the featureless background PL, which is adopted from spectrum A after being scaled to match the low-energy side of each spectrum. (b) PLE spectrum measured by detecting the QD GS emission at the energy of 1.24 eV. (c) A representative PL spectrum from the QD exciton GS with the excitation energy at 1.422 eV. (d) PLE spectra G–I measured by changing the detection energy across the broad QD emission as indicated by the corresponding arrows in (c). The dashed curves are the background PLE spectrum adopted from spectrum I. All spectra are obtained at 5 K and excitation power of 20 mW.

the high-energy side of the PL spectra. They become more apparent from a close comparison with the Gaussian-like line shape shown by the dashed curves in Fig. 2(a) that are derived from spectrum A by scaling it to match the low-energy tail of spectra B-F. With decreasing excitation photon energy, i.e., when E_{exc} is closer to the emission energy, these new features evolve from a weak and structureless shoulder to several pronounced and well-defined resonance peaks. The energies of the resonances are found to change with changing excitation energy, as seen in spectra D-F. This finding safely rules out the QD ES as the origin of the observed resonance peaks since the ES will have their well-defined energy levels regardless of E_{exc}, and they are not expected to be populated under such low excitation density. This conclusion is also supported by the larger number of resonances observed here as compared with that of the ES uncovered from the state filling experiment shown in Fig. 1(c). Consistently, as shown in Fig. 2(d), resonant features are also resolved in PLE spectra G and H obtained under the same experimental conditions when $E_{\mathrm{exc}} < X^{\mathrm{QW}}_{\text{hh-}e}$ by detecting the high-energy side of the QD GS PL band as indicated by the arrows G and H in

Fig. 2(c). These resonant features gain strength and become better resolved when the excitation photon energy is closer to the detected emission energy E_{emi}; a similar trend is seen for the resonance features in the PL spectra shown in Fig. 2(a). When the energy separation between the excitation and detected energy is large [see spectrum I in Fig. 2(d) by monitoring the low-energy QD GS PL band], only a featureless background PLE spectrum is observed.

C. LO-assisted exciton generation

In order to reveal a possible correlation between the excitation and emission photon energy associated with the resonance peaks, we replot the PL and PLE spectra with respect to the difference between the excitation and emission energy $E_{diff} = E_{exc} - E_{emi}$. In addition, we subtract the featureless background PL and PLE spectra represented by the dashed curves in Figs. 2(a) and 2(d), respectively. In doing so, these background contributions (denoted by I^b_{PL}) unrelated to the resonance features (denoted by $I^{LO}_{PL} = I^{total}_{PL} - I^b_{PL}$) are largely removed. Furthermore, in order to take into account the spectrally dependent density-of-states distribution of the QD ensemble that is largely reflected by I^b_{PL}, we normalize I^{LO}_{PL} by I^b_{PL}. The resulting PL and PLE spectra are shown in Figs. 3(a) and 3(b), respectively, which clearly demonstrate that the resonance peaks are closely related to LO phonons. We note that similar behavior has been previously observed and attributed to LO-phonon-assisted energy relaxation in QDs [18,22]. The resonances appear as a consequence of accelerated energy relaxation via emission of LO phonons,

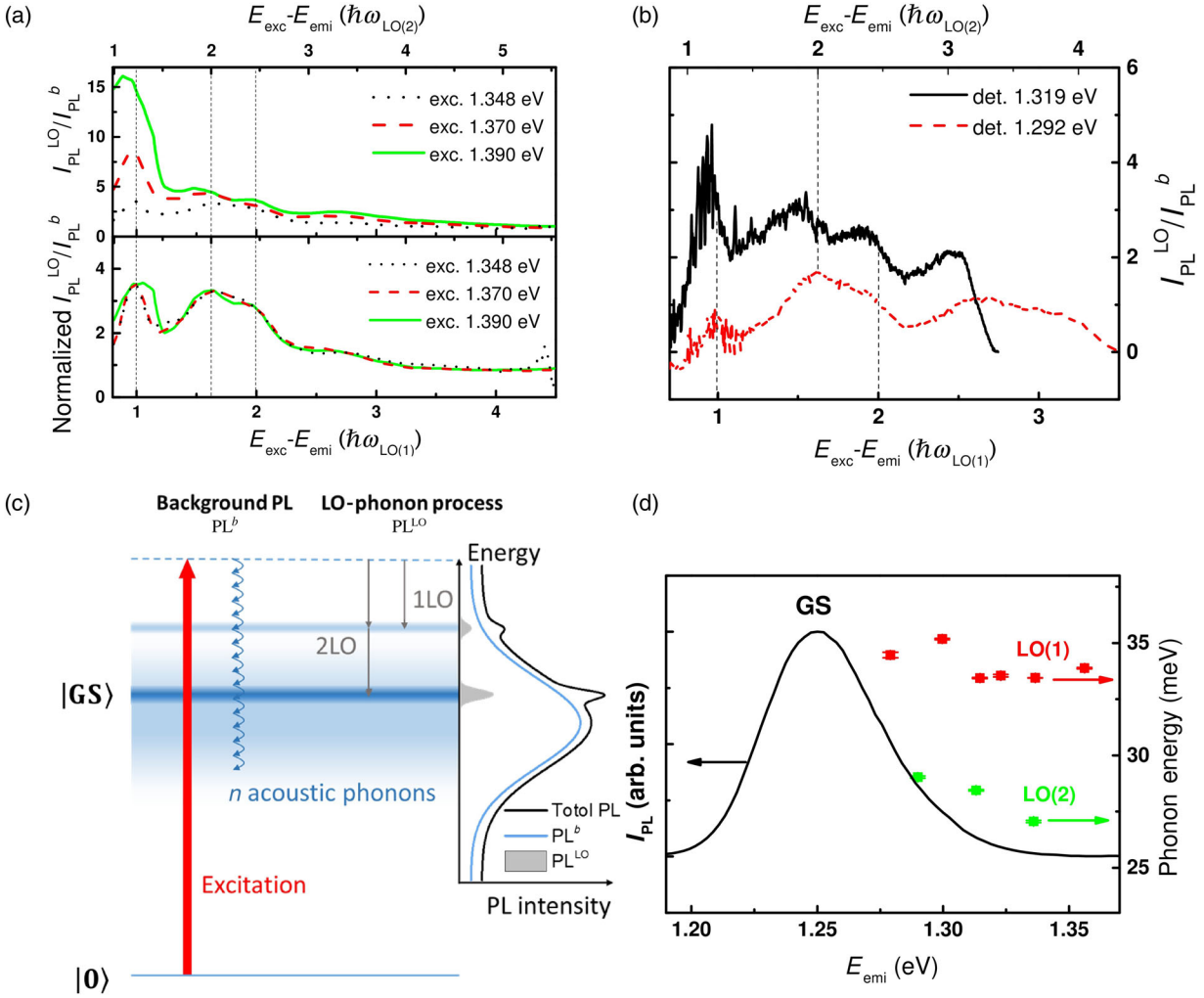

FIG. 3. (a) Normalized PL and (b) PLE intensity, i.e., I^{LO}_{PL}/I^b_{PL}, as a function of $E_{exc} - E_{emi}$, in the units of the phonon energies $\hbar\omega_{LO(1)}$ (35 meV) and $\hbar\omega_{LO(2)}$ (28 meV). The excitation and emission photon energies used in the PL and PLE are given in (a) and (b), respectively. In (a), the upper and lower panels show the PL spectra before and after the QD exciton GS lifetime is taken into account. In (b), only the spectral range up to $X^{QW}_{hh\text{-}e}$ is shown, and the spectra are normalized to the intensity of $X^{QW}_{hh\text{-}e}$ but not calibrated by the lifetime effect of the QD GS. (c) A schematic illustration of the physical processes leading to the background and LO-assisted PL. (d) The energies of the LO(1) and LO(2) phonons as a function of the QD exciton GS energy.

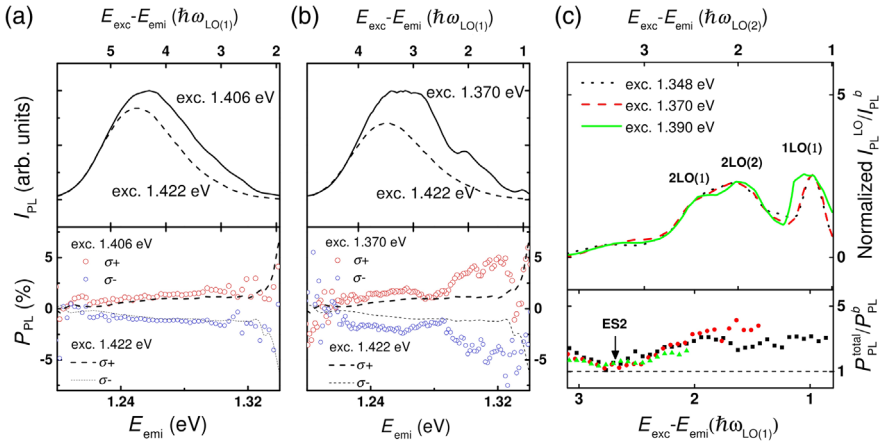

FIG. 4. (a),(b) PL (upper panel) and P_{PL} (lower panels) spectra measured under below-$X_{hh\text{-}e}^{QW}$ excitation with the photon energies of 1.406 and 1.370 eV, respectively. The background PL and P_{PL} spectra obtained under above-$X_{hh\text{-}e}^{QW}$ excitation at 1.422 eV are shown by the dashed curves. (c) I_{PL}^{LO}/I_{PL}^{b} and $P_{PL}^{total}/P_{PL}^{b}$ as a function of $E_{exc}-E_{emi}$ obtained at three different excitation energies.

as schematically illustrated in Fig. 3(c), which is allowed only when the energy difference between the excitation energy and the QD GS matches the energy of an integer number of a specific phonon mode. Indeed, if we now assume two LO-phonon modes, LO(1) and LO(2), the dominant resonances observed in Fig. 3(a) can be assigned to the emissions of 1LO(1), 2LO(2), and 2LO(1). The energies of LO(1) and LO(2) are $\hbar\omega_{LO(1)} = 33.4$–$35.2$ meV and $\hbar\omega_{LO(2)} = 27.1$–$29.0$ meV, which slightly vary with the QD GS energy as shown in Fig. 3(d) and can be attributed to a combined effect of alloy composition, strain, and quantum confinement [23,24]. We note that the resonance feature around 3LO is predominantly contributed from the resonant excitation at the QD excited state ES2, supported by the PL polarization results to be presented in Fig. 4.

We should note that the normalized PL and PLE spectra of the LO resonances (i.e., I_{PL}^{LO}/I_{PL}^{b}) shown in Figs. 3(a) and 3(b) should, in principle, be identical regardless of the excitation (or emission) energies as far as the relative intensity between various LO-phonon resonances is concerned. The observed deviation from such an ideal case can be explained by a difference in the interdot energy transfer efficiency between QDs with different GS energies. It is well known from earlier studies that high-energy QDs suffer more severely than low-energy QDs in energy transfer, leading to a shorter exciton lifetime and a lower steady-state population (thus, weaker PL intensity) for the former. The extent of such lifetime shortening for the high-energy QDs can be reduced under a high excitation density when the low-energy QDs are filled up. The LO resonance peaks in the I_{PL}^{LO}/I_{PL}^{b} spectra shown in Figs. 3(a) and 3(b) result from more efficient exciton generation and, consequently, a reduction in energy transfer, as compared to the background PL and PLE spectra. Therefore, their normalized I_{PL}^{LO}/I_{PL}^{b} intensity tends to be overestimated on the high-energy side of the QD GS emission by a factor of τ^{LO}/τ^{b}, where τ^{LO} and τ^{b} denote the QD GS exciton lifetimes under the excitation condition with and without the accelerated LO-assisted energy relaxation, respectively. This lifetime effect gives rise to the observed stronger 1LO (1) resonance peak with increasing excitation and emission energy shown in Figs. 3(a) and 3(b). It is also largely responsible for the apparent shift of the 1LO(1) and 2LO(2) peaks with increasing excitation energy seen in the upper panel of Fig. 3(a). Corresponding I_{PL}^{LO}/I_{PL}^{b} spectra after taking into account the lifetime effect are shown in the lower panel of Fig. 3(a), which are nearly identical for all excitation energies, as expected. From these calibrated spectra, the exciton generation assisted by the LO phonons can be estimated to be around 3 times more efficient than that suffered from the phonon bottleneck effect. Unfortunately, a similar analysis of the PLE spectra cannot be reliably done due to the complication and uncertainty in the presence of a large contribution from the excited states of the QDs. We note that the observed threefold enhancement in the exciton generation efficiency corresponds to $\tau_{rlx}^{LO-1}/\tau_{rlx}^{b-1} = 3$. Here, τ_{rlx}^{LO} and τ_{rlx}^{b} are the relaxation times of the LO-assisted process and the phonon bottleneck process involving emission of multiple acoustic phonons. If we assume τ_{rlx}^{b} to be similar to the typical value of 500 ps to 1 ns reported for the energy relaxation time relevant to the phonon bottleneck channel in similar self-assembled QD systems [19,25,26], τ_{rlx}^{LO} can be estimated to be of the order of a few hundred picoseconds.

D. Origin of the LO phonons

The LO(1) phonon energy is comparable with the typical values of 33–35 meV reported for the LO-phonon energy in strained $In_{1-x}Ga_xAs/GaAs$ QDs, which originates from the Γ point of the phonon dispersion [27–29]. On the other hand, the energy of the LO(2) phonon resonances coincides with the LO-phonon mode at the boundary of the Brillouin zone [30]. Here, we adopt the concept of phonon dispersion from a bulk crystal, which is still valid as the phonon confinement effect is expected to be negligibly weak for QDs of the size similar to our QDs [31]. Interestingly, we notice that the scattering process involving the zone-edge LO(2) phonons in our QDs seems to be significant only when they are emitted in pairs, whereas at the energy of 1LO(2), no resonance is

observable within our detection limit. This "selection rule" is required typically in a higher-dimensional system with energy-momentum dispersion by conservation of momentum before and after phonon scattering. While the zone-center phonon LO(1) introduces no change of exciton momentum, the momentum-conservation process requires the involvement of two zone-edge LO(2) by scattering first across the Brillouin zone and then back. In an ideal picture, a QD with a strong three-dimensional confinement in real space should result in a wide spread in the momentum space such that the momentum conservation should be largely relaxed. The momentum conservation observed in our QDs probably arises from a finite lateral confinement of our QD samples. It is well established for self-assembled QDs that, although the vertical confinement is strong, the lateral confining potential is often weak and can be approximated by a parabolic shape, resulting in the famous Fock-Darwin states with a limited spread of its momentum [32]. Following a simple estimation from the uncertainty principle, the 20 nm lateral diameter of a QD actually corresponds to momentum uncertainty that is about 3 orders of magnitude smaller than the Brillouin zone size of InAs. This means that the QD states are mainly localized at the center of the Brillouin zone, which imposes a certain degree of the momentum conservation during phonon-assisted energy relaxation within the QDs.

E. Optical spin orientation

To examine the effect of the energy relaxation processes on spin generation in the studied QDs, we conduct optical orientation experiments in which exciton spins are generated by circularly polarized excitation light following the well-known optical selection rule [33]. Thanks to the quantum confinement and compressive strain experienced in the QDs and the QW grown on a GaAs substrate, the excitonic GS in the QDs and QW is expected to be predominantly of a heavy-hole character, with a light-hole (LH) contribution of less than 7% for the QDs [34] and negligible for the QW. This enables the generation of electron and exciton spin polarization in both QW and QDs. For example, σ^- excitation is expected to create an exciton ($|M_J^{\rm ex}=-1\rangle = |m_s^e=\frac{1}{2},\ m_j^h=-\frac{3}{2}\rangle$) with a fully polarized spin-up electron and a spin-down hole, whereas the σ^+ excitation does the opposite. Here, $M_J^{\rm ex}$, m_s^e, and m_j^h denote the magnetic quantum numbers of the exciton, and the electron and hole of the exciton, respectively. The same selection rule applies to the circular polarization of the PL emission from the QD exciton GS, giving rise to a one-to-one correspondence between the optical and exciton spin polarization, i.e., $P_{\rm PL}=P_{\rm ex}$. By measuring the circular polarization degree of the QD excitonic GS emission, therefore, spin depolarization occurring during the energy relaxation process and also during the exciton lifetime can be assessed. (It is commonly accepted that due to strong spin-orbit coupling and HH-LH mixing, a hole suffers more severe spin depolarization than an electron, and the exciton spin polarization is mainly determined by the electron spin polarization P_e such that $P_{\rm ex}=-P_e$.)

In Figs. 4(a) and 4(b), PL intensity ($I_{\rm PL}$) and PL polarization ($P_{\rm PL}$) spectra are plotted and compared between the excitation energies that are above (at 1.422 eV) and below (at 1.406 and 1.370 eV) $X_{\text{hh-}e}^{\rm QW}$. The excitation power is scaled such that the same total PL intensity is obtain in all cases. This ensures that the total number of excitons generated in the QDs is similar regardless of the excitation photon energies, such that any dynamic charging effect that may arise from different excitation power densities can be suppressed [35,36]. Under the excitation at 1.406 eV, which is below $X_{\text{hh-}e}^{\rm QW}$ but still high above the QD GS emission when the higher-order LO-phonon resonances just start to emerge in the PL spectrum [see Fig. 4(a)], only a slight increase of $|P_{\rm PL}|$ is detected as compared with that of the background PL obtained under above $X_{\text{hh-}e}^{\rm QW}$ excitation at 1.422 eV. When the excitation photon energy is tuned closer to the QD GS emission, the lower-order LO-phonon resonances also appear and become dominate in the PL spectrum as shown in Fig. 4(b). This emerging resonance feature is accompanied by a sizable enhancement in $|P_{\rm PL}|$ at the LO-phonon resonances.

F. LO-assisted spin generation

The measured $P_{\rm PL}$ and, thus, $P_{\rm ex}$ (or P_e) are a product of spin-generation efficiency P_0 and spin-conserving factor (or spin-detection efficiency) $P_d=[1/(1+\tau/\tau_s)]$ in the QD exciton GS, i.e., $P_{\rm PL}=P_0P_d$. As P_d is determined by the exciton lifetime τ and spin lifetime τ_s that are independent of excitation photon energy for a given QD, the effect of the phonon bottleneck on the spin-generation efficiency P_0 alone can, thus, be singled out by the ratio between the PL polarization degree under the conditions with and without the LO-assisted energy relaxation. Namely, $(P_0^{\rm LO}/P_0^b)=(P_{\rm PL}^{\rm LO}/P_{\rm PL}^b)$, which is independent of spin loss of the QDs during the lifetime of the exciton GS. To avoid the uncertainty in separating polarization components between the LO-assisted resonances and the background PL band and possible errors it may introduce, we choose to analyze the polarization ratio $P_{\rm PL}^{\rm total}/P_{\rm PL}^b$ between the total PL and the background PL that is a measure of $P_0^{\rm LO}/P_0^b$ following the relationship $(P_{\rm PL}^{\rm LO}/P_{\rm PL}^b)=(P_{\rm PL}^{\rm total}/P_{\rm PL}^b)+(1/\beta)[(P_{\rm PL}^{\rm total}/P_{\rm PL}^b)-1]$, where $\beta=(I_{\rm PL}^{\rm LO}/I_{\rm PL}^b)$. The resulting $P_{\rm PL}^{\rm total}/P_{\rm PL}^b$ as a function of the LO resonance is shown in the lower panel of Fig. 4(c), which is greater than 1 throughout the LO resonances, meaning $(P_{\rm PL}^{\rm LO}/P_{\rm PL}^b)>(P_{\rm PL}^{\rm total}/P_{\rm PL}^b)>1$. In other words, $P_{\rm PL}^{\rm LO}>P_{\rm PL}^{\rm total}$, implying that $P_{\rm PL}^{\rm total}$ provides the low bound of $P_{\rm PL}^{\rm LO}$. These results provide compelling experimental evidence that the LO-assisted accelerated exciton generation leads to more efficient exciton (and electron) spin generation, at least by a factor of 2–3 for the low-order LO resonances. We note that the dip in $P_{\rm PL}^{\rm total}/P_{\rm PL}^b$ (indicated

by the arrow marked by ES2) corresponds to poor spin generation under the resonant excitation at the excited state ES2 of the QDs. Though the exact reason for this reduction is currently unknown, which is beyond the scope of the present study, we speculate that it could probably arise from the effect of spin blockade and spin-flip relaxation from the ES2 to the GS [37,38]. The observed ES2-related $P_{\mathrm{PL}}^{\mathrm{total}}/P_{\mathrm{PL}}^{b}$ dip also implies that the exciton generation via the resonant excitation at the ES2 is the predominant contribution over the corresponding spectral range of the $I_{\mathrm{PL}}^{\mathrm{LO}}/I_{\mathrm{PL}}^{b}$ spectra, leading to a large uncertainty in estimating the LO resonances in the PL and PL polarization beyond the 2LO phonons. Therefore, only results from the 1LO and 2LO resonances are regarded as reliable here. We note that a similar enhancement of the PL polarization is observed in all studied samples regardless of the tunneling barrier thickness. This is expected as the LO-phonon-assisted exciton and spin-generation process do not involve the tunneling injection from the QW and are the intrinsic properties of the QDs.

We note here that phonon scattering alone should, in principle, conserve spins. The observed different degrees of spin losses between the LO-assisted and acoustic phonon-exciton generation monitored by the LO resonant features and the background PL, should, thus, originate from a higher-order effect in which the exciton-phonon interactions are coupled with spin-flipping mechanisms such as spin-orbit interactions, hyperfine coupling, etc. At present, the exact physical mechanisms for the observed spin losses remain unknown, which requires future theoretical and experimental studies.

G. Temperature dependence of the LO-assisted spin generation

The temperature dependence of P_{PL} is measured under the excitation condition with or without the LO-assisted energy relaxation process from 6 to 90 K until the phonon structures broaden beyond recognition. The excitation photon energy at 6 K is set at 1.370 and 1.422 eV for the excitation condition $E_{\mathrm{exc}} < X_{\mathrm{hh}\text{-}e}^{\mathrm{QW}}$ and $E_{\mathrm{exc}} > X_{\mathrm{hh}\text{-}e}^{\mathrm{QW}}$, respectively. They are adjusted when the temperature increases, following a redshift of the QD GS PL emission. This is to ensure that the optical spin orientation is performed approximately on the same exciton state of the QDs or the QW, such that the obtained temperature dependence is meaningful. In Fig. 5(a), we display representative results of $P_{\mathrm{PL}}^{\mathrm{total}}/P_{\mathrm{PL}}^{b}$ at 15, 45, and 75 K. The full temperature dependence is shown in Fig. 5(b). It clearly demonstrates that the enhancement in spin-generation efficiency achieved via the LO-phonon emission is robust against the temperature and remains sizable at 75 K. It is highly likely that the phonon bottleneck effect remains active at even higher temperatures, even though the LO-phonon features can no longer be resolved due to the broadening effect.

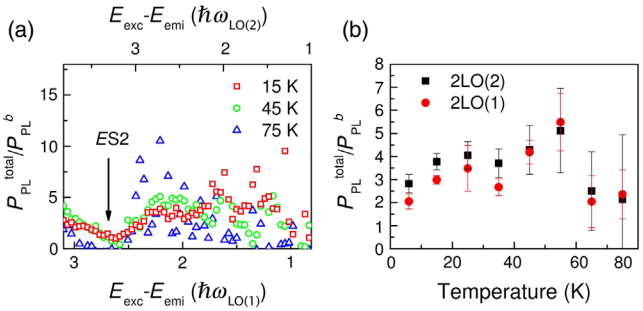

FIG. 5. (a) $P_{\mathrm{PL}}^{\mathrm{total}}/P_{\mathrm{PL}}^{b}$ as a function of $E_{\mathrm{exc}} - E_{\mathrm{emi}}$ measured at 15, 45, 75 K. (b) Temperature dependence of $P_{\mathrm{PL}}^{\mathrm{total}}/P_{\mathrm{PL}}^{b}$ from the 2LO(1) and 2LO(2) resonances. The excitation photon energies of 1.370 and 1.422 eV are used at 6 K to obtain the data related to the LO-assisted and background PL, respectively. They are adjusted at elevated temperatures following the redshift of the PL emission to ensure the same QD exciton GS is monitored at different temperatures.

IV. SUMMARY

We experimentally demonstrate a sizable phonon bottleneck effect on both exciton and spin-generation efficiency in self-assembled $In_{0.5}Ga_{0.5}As$ QD nanostructures. We show that QD exciton generation accelerated by the LO-assisted energy relaxation, which overcomes the phonon bottleneck, is at least 3 times more efficient than the acoustic phonon-assisted generation process that suffers from the phonon bottleneck effect. More interesting, the circular polarization of the QDs emission increases from 2% to approximately 5% when the phonon bottleneck effect is suppressed, leading to an enhancement of spin-generation efficiency by a similar factor. Such an enhancement remains effective even at elevated temperatures. These findings not only identify the phonon bottleneck effect as an important obstacle in exciton and spin generation, but they also suggest a pathway for further improvements in the performance of QD-based light-emitting and spintronic devices (e.g., QD spin LEDs or polarized light sources) toward both high emission intensity and a high optical (spin) polarization degree by carefully engineering the energies of the QDs and their excitation channels.

ACKNOWLEDGMENTS

This work is supported by Linköping University through the Professor Contracts, the Swedish Research Council (Grants No. 621-2011-4254 and No. 2016-05091), the Swedish Government Strategic Research Area in Materials Science on Functional Materials at Linköping University (Faculty Grant SFO-Mat-LiU No. 2009-00971), the Swedish Foundation for International Cooperation in Research and Higher Education (STINT) (Grant No. JA2014-5698), the Japan Society for the Promotion of Science, Grant-in-Aid for Scientific Research (S) No. 16H06359, and the Bilateral Joint Research Project.

[1] Y. Arakawa and H. Sakaki, Multidimensional quantum well laser and temperature dependence of its threshold current, Appl. Phys. Lett. **40**, 939 (1982).

[2] L. Goldstein, F. Glas, J. Y. Marzin, M. N. Charasse, and G. Le Roux, Growth by molecular beam epitaxy and characterization of InAs/GaAs strained-layer superlattices, Appl. Phys. Lett. **47**, 1099 (1985).

[3] R. C. Ashoori, H. L. Stormer, J. S. Weiner, L. N. Pfeiffer, S. J. Pearton, K. W. Baldwin, and K. W. West, Single-Electron Capacitance Spectroscopy of Discrete Quantum Levels, Phys. Rev. Lett. **68**, 3088 (1992).

[4] U. Banin, Y. Cao, D. Katz, and O. Millo, Identification of atomic-like electronic states in indium arsenide nanocrystal quantum dots, Nature (London) **400**, 542 (1999).

[5] Q. Sun, Y. A. Wang, L. S. Li, D. Y. Wang, T. Zhu, J. Xu, C. H. Yang, and Y. F. Li, Bright, multicoloured light-emitting diodes based on quantum dots, Nat. Photonics **1**, 717 (2007).

[6] D. Bimberg, N. Kirstaedter, N. N. Ledentsov, Z. I. Alferov, P. S. Kop'ev, and V. M. Ustinov, (In,Ga)As-GaAs quantum-dot lasers, IEEE J. Sel. Top. Quantum Electron. **3**, 196 (1997).

[7] S. Strauf, N. G. Stoltz, M. T. Rakher, L. A. Coldren, P. M. Petroff, and D. Bouwmeester, High-frequency single-photon source with polarization control, Nat. Photonics **1**, 704 (2007).

[8] D. Huber, M. Reindl, Y. Huo, H. Huang, J. S. Wildmann, O. G. Schmidt, A. Rastelli, and R. Trotta, Highly indistinguishable and strongly entangled photons from symmetric GaAs quantum dots, Nat. Commun. **8**, 15506 (2017).

[9] M. I. Dyakonov, *Spin Physics in Semiconductors*, 1st ed. (Springer Berlin, 2008).

[10] R. Oulton, A. Greilich, S. Y. Verbin, R. V. Cherbunin, T. Auer, D. R. Yakovlev, M. Bayer, I. A. Merkulov, V. Stavarache, D. Reuter, and A. Wieck, Subsecond Spin Relaxation Times in Quantum Dots at Zero Applied Magnetic Field Due to a Strong Electron-Nuclear Interaction, Phys. Rev. Lett. **98**, 107401 (2007).

[11] A. Bechtold, D. Rauch, F. Li, T. Simmet, P.-L. Ardelt, A. Regler, K. Müller, N. A. Sinitsyn, and J. J. Finley, Three-stage decoherence dynamics of an electron spin qubit in an optically active quantum dot, Nat. Phys. **11**, 1005 (2015).

[12] M. Atature, J. Dreiser, A. Badolato, A. Hogele, K. Karrai, and A. Imamoğlu, Quantum-dot spin-state preparation with near-unity fidelity, Science **312**, 551 (2006).

[13] R. Hanson, L. H. Willems van Beveren, I. T. Vink, J. M. Elzerman, F. H. L. Koppens, L. P. Kouwenhoven, and L. M. K. Vandersypen, Single-shot readout of electron spins in a semiconductor quantum dot, Physica (Amsterdam) **34E**, 1 (2006).

[14] D. D. Awschalom, L. C. Bassett, A. S. Dzurak, E. L. Hu, and J. R. Petta, Quantum spintronics: Engineering and manipulating atom-like spins in semiconductors, Science **339**, 1174 (2013).

[15] M. Holub and P. Bhattacharya, Spin-polarized light-emitting diodes and lasers, J. Phys. D **40**, R179 (2007).

[16] H. Benisty, C. M. Sotomayor-Torrès, and C. Weisbuch, Intrinsic mechanism for the poor luminescence properties of quantum-box systems, Phys. Rev. B **44**, 10945 (1991).

[17] B. Ohnesorge, M. Albrecht, J. Oshinowo, A. Forchel, and Y. Arakawa, Rapid carrier relaxation in self-assembled $In_xGa_{1-x}As/GaAs$ quantum dots, Phys. Rev. B **54**, 11532 (1996).

[18] H. Kumano, H. Yoshida, T. Tawara, and I. Suemune, Longitudinal-optical-phonon-assisted energy relaxation in self-assembled CdS quantum dots embedded in ZnSe, J. Appl. Phys. **92**, 3573 (2002).

[19] J. Urayama, T. B. Norris, J. Singh, and P. Bhattacharya, Observation of Phonon Bottleneck in Quantum Dot Electronic Relaxation, Phys. Rev. Lett. **86**, 4930 (2001).

[20] X.-J. Yang, T. Kiba, T. Yamamura, J. Takayama, A. Subagyo, K. Sueoka, and A. Murayama, Ultrafast spin tunneling and injection in coupled nanostructures of (In,Ga)As quantum dots and quantum well, Appl. Phys. Lett. **104**, 012406 (2014).

[21] S. L. Chen, T. Kiba, X. J. Yang, J. Takayama, and A. Murayama, Temperature-dependent spin injection dynamics in InGaAs/GaAs quantum well-dot tunnel-coupled nanostructures, J. Appl. Phys. **119**, 115701 (2016).

[22] R. Heitz, M. Veit, N. N. Ledentsov, A. Hoffmann, D. Bimberg, V. M. Ustinov, P. S. Kop'ev, and Z. I. Alferov, Energy relaxation by multiphonon processes in InAs/GaAs quantum dots, Phys. Rev. B **56**, 10435 (1997).

[23] T. P. Pearsall, R. Carles, and J. C. Portal, Single longitudinal-mode optical phonon scattering in $Ga_{0.47}In_{0.53}As$, Appl. Phys. Lett. **42**, 436 (1983).

[24] J. Groenen, C. Priester, and R. Carles, Strain distribution and optical phonons in InAs/InP self-assembled quantum dots, Phys. Rev. B **60**, 16013 (1999).

[25] K. Ikeda, H. Sekiguchi, F. Minami, J. Yoshino, Y. Mitsumori, H. Amanai, S. Nagao, and S. Sakaki, Phonon bottleneck effects in InAs/GaInP quantum dots, J. Lumin. **108**, 273 (2004).

[26] K. Mukai, N. Ohtsuka, H. Shoji, and M. Sugawara, Phonon bottleneck in self-formed $In_xGa_{1-x}As/GaAs$ quantum dots by electroluminescence and time-resolved photoluminescence, Phys. Rev. B **54**, R5243 (1996).

[27] T. Inoshita and H. Sakaki, Electron relaxation in a quantum dot: Significance of multiphonon processes, Phys. Rev. B **46**, 7260 (1992).

[28] X.-Q. Li, H. Nakayama, and Y. Arakawa, Phonon bottleneck in quantum dots: Role of lifetime of the confined optical phonons, Phys. Rev. B **59**, 5069 (1999).

[29] Y. I. Mazur, Z. M. Wang, G. J. Salamo, V. V. Strelchuk, V. P. Kladko, V. F. Machulin, M. Y. Valakh, and M. O. Manasreh, Investigation of indium distribution in InGaAs/GaAs quantum dot stacks using high-resolution x-ray diffraction and Raman scattering, J. Appl. Phys. **99**, 023517 (2006).

[30] T. B. Boykin, A. Ajoy, H. Ilatikhameneh, M. Povolotskyi, and G. Klimeck, Brillouin zone unfolding method for effective phonon spectra, Phys. Rev. B **90**, 205214 (2014).

[31] X.-Q. Li and Y. Arakawa, Confined optical phonons in semiconductor quantum dots, Solid State Commun. **109**, 351 (1999).

[32] S. Raymond, S. Studenikin, A. Sachrajda, Z. Wasilewski, S. J. Cheng, W. Sheng, P. Hawrylak, A. Babinski, M. Potemski, G. Ortner, and M. Bayer, Excitonic Energy Shell Structure of Self-Assembled InGaAs/GaAs Quantum Dots, Phys. Rev. Lett. **92**, 187402 (2004).

[33] F. Meier and B. P. Zakharchenya *Optical Orientation* (North-Holland, Amsterdam, 1984).

[34] G. A. Narvaez, G. Bester, and A. Zunger, Dependence of the electronic structure of self-assembled $(\mathrm{In,Ga})\mathrm{As}/\mathrm{GaAs}$ quantum dots on height and composition, J. Appl. Phys. **98**, 043708 (2005).

[35] Y. Q. Huang, Y. Puttisong, I. a. Buyanova, X. J. Yang, A. Subagyo, K. Sueoka, a. Murayama, and W. M. Chen, Size dependence of electron spin dephasing in InGaAs quantum dots, Appl. Phys. Lett. **106**, 093109 (2015).

[36] Y. Puttisong, Y. Q. Huang, I. A. Buyanova, X. J. Yang, A. Subagyo, K. Sueoka, A. Murayama, and W. M. Chen, Anomalous spectral dependence of optical polarization and its impact on spin detection in InGaAs/GaAs quantum dots, Appl. Phys. Lett. **105**, 132106 (2014).

[37] I. V. Ignatiev, S. Y. Verbin, I. Y. Gerlovin, R. V. Cherbunin, and Y. Masumoto, Negative circular polarization of InP QD luminescence: Mechanism of formation and main regularities, Opt. Spectrosc. **106**, 375 (2009).

[38] S. Cortez, O. Krebs, S. Laurent, M. Senes, X. Marie, P. Voisin, R. Ferreira, G. Bastard, J.-M. Gérard, and T. Amand, Optically Driven Spin Memory in *n*-Doped InAs-GaAs Quantum Dots, Phys. Rev. Lett. **89**, 207401 (2002).